Proposal to perform an experiment at the A2 hall, MAMI:

"High Precision Measurement of the ep elastic cross section at small Q^2"

Contact person for the Experiment:

Alexey Vorobyev, Petersburg Nuclear Physics Institute
Mainz contact person: Achim Denig, Institute for Nuclear Physics, JGU Mainz

Abstract

This experiment is motivated by the observed striking difference (4%) in the proton radius value extracted from elastic ep scattering and from muonic Lamb shift experiments ("proton radius puzzle"). The proposed experiment aims for a high resolution, high precision measurement of the differential ep elastic cross section in the region of low momentum transfer: $0.001 \leq Q^2 \leq 0.04$ GeV^2. More than 100 resolved experimental points will be obtained in this region with 0.1% point-to-point and 0.2% absolute precision in dσ/dt. This will allow extracting the proton radius with 0.6% precision, which could be decisive in solving the "proton radius puzzle".

The experiment will be performed with a low-intensity, high-precision electron beam at MAMI. An active hydrogen target - specially developed for this experiment - detecting recoil protons will be used in combination with a high precision tracker detecting the scattered electrons. This device allows to measure the recoil proton energy, the recoil proton angle, and the angle of the scattered electron.

The advantages of the proposed experimental method are well determined thickness of a hydrogen gas target without any wall-effects, direct determination of Q^2 by the energy of the recoiled proton, high Q^2 resolution and effective selection of the ep elastic scattering events from the background, absolute measurement of the ep differential cross section. A unique feature of the recoil proton method is relatively low radiative corrections which, together with absolute measurements of dσ/dt, allows to minimize the systematic errors in determination of the proton radius.

The LOI was presented at the PAC meeting in November 2016. Since then, considerable progress was achieved in development of the project. In particular, as it was foreseen in the LOI, a test run was conducted in the 720 MeV electron beam at MAMI using the existing prototype of the hydrogen active target. This run was a success. First, it was demonstrated that MAMI can provide the electron beam with the parameters required for this experiment. Second, it was shown that the background generated in the active target when placed in the electron beam is quite low, such that the target could be operated with the designed parameters. In particular, it was shown that the TPC self-trigger can be used to trigger the read out of the whole system. This is the most effective and reliable trigger option.

The active target used in the test run was filled with the $^4He+4\%N_2$ gas mixture because of restrictions to use hydrogen for the setup available by that time. Though the ionization properties of this gas mixture are quite similar to those of hydrogen, we propose to repeat these measurements in the fall of 2018 with hydrogen in the active target with all the safety measures taken into account. Also, new fast beam detectors could be tested and calibrated in this test run. The full setup for the main experiment should be ready for installation in the experimental hall in the fall of 2019.

MAMI Specifications

Beam energy	720 MeV
Energy spread	< 20 keV (1σ)
Energy shift	< 20 keV (1σ)
Absolute energy	±< 150 keV (1 σ)

Electron Beam Specifications

Beam intensity (main run)	2x10^6 e/sec
Beam intensity for calibration	10^4 e/sec and 10^3 e/sec
Beam divergency	≤ 0.5 mrad
Beam size	minimal at given divergence

Beam Time Request

2018

Test run with prototype of the active target (hydrogen filling). 3 weeks

2019

Test run with full setup. 3 weeks

2020

Physics run. 6 weeks

1. Introduction

The striking difference in the proton radius values extracted from the elastic ep scattering experiments (Rp =0.877 (5)) and from the muonic Lamb shift experiments (Rp = 0.8409 (4)) is widely discussed in scientific community [1]. It is generally agreed that new experiments are needed to resolve this puzzle. In particular, new high precision measurements of differential cross sections of the ep elastic scattering in the low Q^2 region are important.

The ep elastic scattering differential cross section is given by the following expression:

$$\frac{d\sigma}{dt} = \frac{\pi\alpha^2}{t^2}\left\{G_E^2\left[\frac{(4M + t/\varepsilon_e)^2}{4M^2 - t} + \frac{t}{\varepsilon_e^2}\right] - \frac{t}{4M^2}G_M^2\left[\frac{(4M + t/\varepsilon_e)^2}{4M^2 - t} - \frac{t}{\varepsilon_e^2}\right]\right\} \qquad (1)$$

where $t = -Q^2$, $\alpha = 1/137$, ε_e - initial electron energy, M – proton mass, G_E – electric form factor, and G_M – magnetic form factor.

At low Q^2 the form factors can be represented by the expansions:

$$\frac{G(Q^2)}{G(0)} = 1 - \frac{1}{6}\langle R_p^2\rangle Q^2 + \frac{1}{120}\langle R_p^4\rangle Q^4 - \ldots, \qquad (2)$$

The electric proton radius R_{pE} can be measured by measuring the slope of the electric form factor G_E as Q^2 goes to zero:

$$R_{pE}^2 = -6 \cdot \frac{dG_E(Q^2)}{dQ^2}\bigg|_{Q^2 \to 0} \qquad (3)$$

An example of dσ/dt in the small Q^2 region is shown in Fig 1.

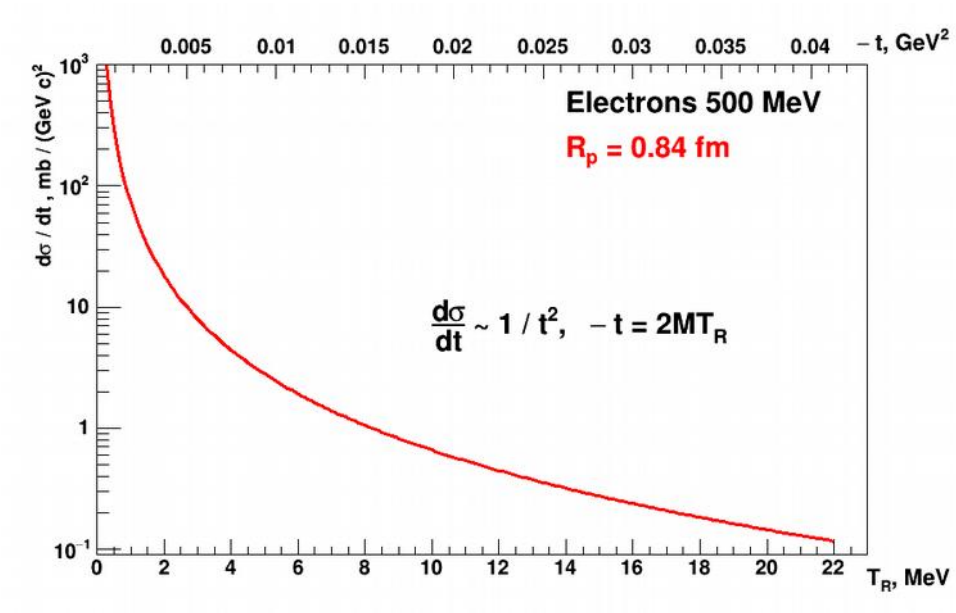

Fig.1. *Differential cross section of the ep elastic scattering calculated for ε_e =500 MeV with electric and magnetic form factors represented by expansion (3).*

The region of $Q^2 \le 0.02$ GeV² seems to be optimal for such measurements as the nonlinear effects, essential at higher transfer momenta, should not be signiificant in

this region. Also, the contribution of magnetic scattering is quite small. On the other hand, the sensitivity of dσ/dt to the proton radius at $Q^2 \leq 0.02$ GeV^2 is rather small as it is demonstrated in Fig 2. This figure shows the ratio of dσ/dt calculated for two different values of Rp to that calculated for the point-like proton. The cross sections corresponding to Rp =0.88 fm and Rp=0.84 fm differ only by 1.3% at $Q^2 = 0.02$ GeV^2 (Fig.3). That means that at least 0.2% precision in measurements of dσ/dt in the region $Q^2 \leq 0.02$ GeV^2 is needed to distinguish reliably these two options.

As to the lowest Q^2, it could be 0.001-0.002 GeV^2 where the difference in dσ/dt corresponding to the considered two options of the proton radius (Rp =0.88 fm and Rp=0.84 fm) becomes negligible (0.065% - 0.13%, respectively).

The measurements need high Q^2 resolution to have as many resolved points in the studied Q^2 region as possible – this would be an important control for the $G_E(Q^2)$ linearity.

The measurements of the slope in $G_E(Q^2)$ could be relative, that is without absolute normalization of dσ/dt, as it was in all previous measurements, but it is **highly desirable to have absolute measurements of dσ/dt**. In this case, the measured $(d\sigma/dt)_{expt}$ could be directly compared with the theoretical $(d\sigma/dt)_{theory}$ (after applying the radiative corrections) thus providing control over the calculated radiative corrections and making measurements of the proton radius more reliable.

The radiative corrections are an essential factor in the ep-scattering. Depending on the experimental conditions, they may change dσ/dt by ~10%, as it was in the previous measurements. Moreover, this corrections depend on Q^2, thus influencing directly on the slope of the extracted form factor, that is on the value of the proton radius.

An important advantage of the recoil proton method, expolited in this project for the first time in the ep scattering experiments, is that the radiative corrections are strongly reduced in this case.

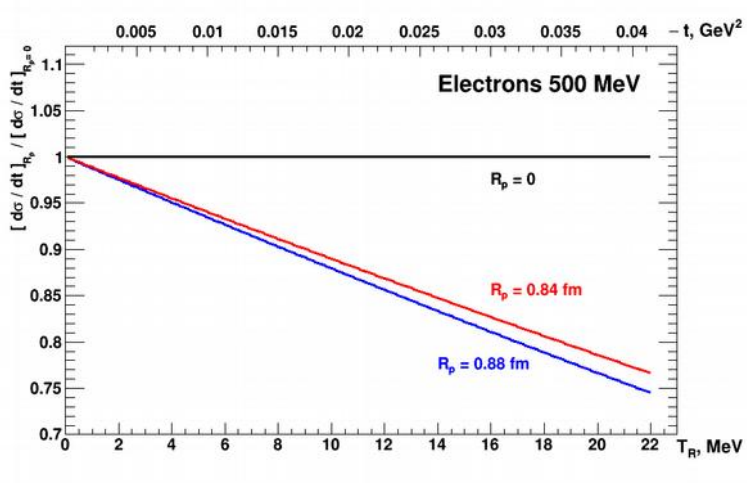

Fig.2. *Ratio of dσ/dt calculated for two different values of Rp to that calculated for the point-like proton.*

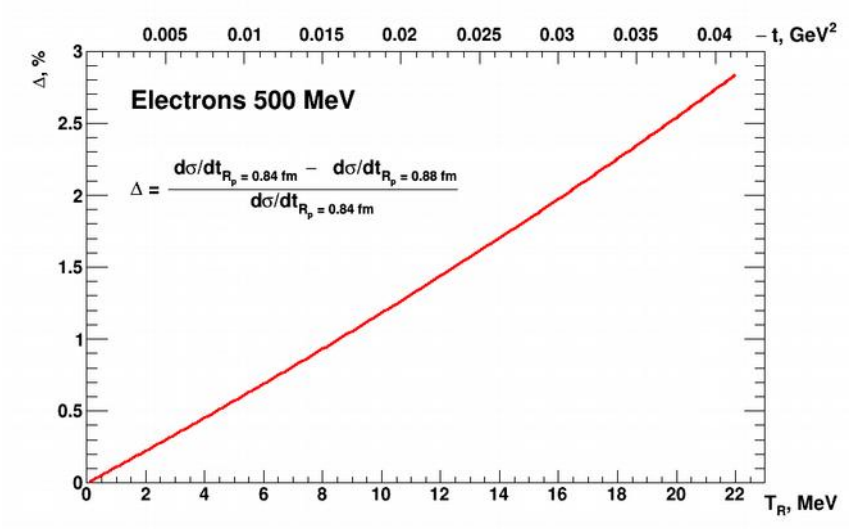

Fig.3. *Difference between the ep differential cross sections corresponding to Rp=0.84 fm and Rp=0.88 fm.*

The requirements to the new generation measurements of the proton radius in ep scattering experiments could be summarized as follows:

- Low transfer momentum region, 10^{-3} GeV$^2 \leq Q^2 \leq 2 \cdot 10^{-2}$ GeV^2;
- High resolution in Q^2;
- Absolute measurements of dσ/dt with 0.2% precision;
- Control for the radiative corrections.

The first experiment designed to meet such requirements is the PRad experiment at Jefferson laboratory. This experiment studies the electron scattering on the hydrogen gas jet target. The transfer momentum is determined by the electron scattering angle, the energy of the scattered electron is measured by a calorimeter, the measured ep cross sections are normalized to the simultaneously measured Møller cross section. The PRad experiment was approved in 2012, and it began data taking in 2016.

The experiment presented in our proposal has similar goals but it is based on a different experimental method. Therefore, these two experiments will be complementary to each other, thus increasing the confidence in the obtained results.

2. Experimental overview

An active hydrogen target - Time Projection Chamber (**TPC**) - detecting recoil protons will be used in combination with a high precision tracker detecting the scattered electrons. Fig.4 shows a schematic view of the proposed experimental setup. It contains hydrogen TPC and a MWPC based Forward Tracker (**FT**).

The TPC operates in the ionization mode (no gas amplification). It allows to measure: the recoil proton energy T_R, the recoil proton angle θ_R, and the z -coordinate of the vertex Z_V. The x- and y- coordinates are fluctuations around the central values X_V=0 and Y_V=0 determined by the beam position along the TPC axis, the fluctuations being caused by the beam size, beam divergence, and by the Coulomb scattering.

The FT consists of two pairs of Cathode Strip Chambers (**CSC**) X_1/Y_1 and X_2/Y_2 interspaced by 100 mm. The CSCs measure the X_1/Y_1 and X_2/Y_2 coordinates of the scattered electrons. The scattering angle θ_e is determined using the $Z_V/X_V/Y_V$ and X_1/Y_1 coordinates (the main mode) or X_1/Y_1 and X_2/Y_2 coordinates (complimentary mode).

Outside the volume of the main detector, fast scintillator detectors are placed to determine the beam electron arrival times and provide absolute counting rate of the beam electrons for measurements of the absolute cross section. Also, pixel detectors will be used for determination of the beam axis and for control for the beam position stability in the course of the measurements.

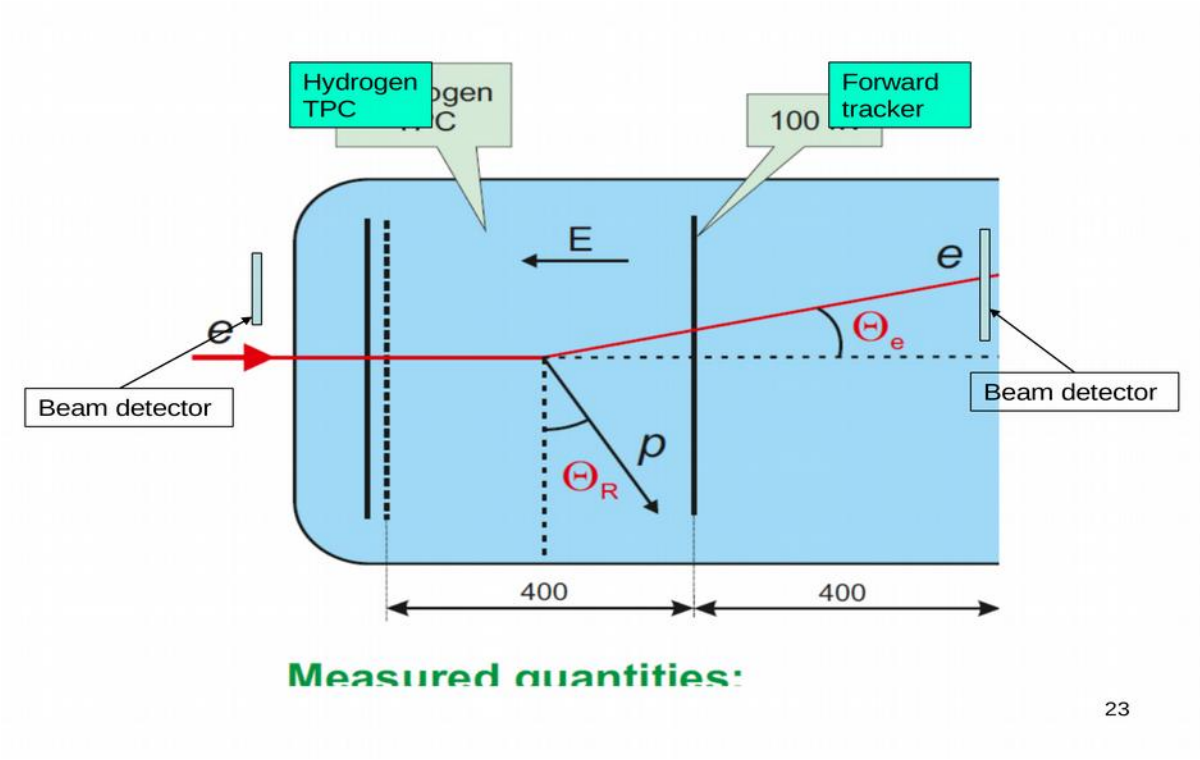

Fig. 4. *Schematic view of the combined TPC & FT detector.*

The transfer momentum –t, can be determined either by the recoil proton energy T_R or from the electron scattering angle θ_e. An advantage of the T_R method is that it determines the transfer momentum independently of the electron energy ε_e:

$$-t = 2MT_R . \qquad (4)$$

On the other hand, the ep differential cross section is practically independent on the electron energy at $\varepsilon_e \geq 500$ MeV in the considered low Q^2 region. Therefore, measurements of $d\sigma/dt$ by the T_R method are not sensitive to possible uncertainties in the electron energy. This is especially important for the ep scattering. Note that already after 0,5 mm Be (which is the thickness of the TPC entrance window) the energy tail contains 2%, 0.9%, 0.7%, 0.3 %, and 0.2% of the beam intensity with the energy losses more than 1 MeV, 5 MeV, 10 MeV, 50 MeV, and 100 MeV, respectively, for 500 MeV electrons (Fig.5). In addition, there will be some more materials: beam detectors, hydrogen in TPC. This means that the energy of electrons in the collision point might be essentially different from the initial beam energy. However, *by measuring the transfer momentum by the T_R method, we avoid the influence of the beam energy losses before the ep collision (as well as the initial beam uncertainties) on the measured $d\sigma/dt$.*

On the contrary, the transfer momentum determined via the electron scattering angle θ_e depends on ε_e :

$$-t = \frac{4\varepsilon_e^2 \sin^2\frac{\vartheta}{2}}{1+\frac{2\varepsilon_e}{M}\sin^2\frac{\vartheta}{2}} \qquad (5)$$

Therefore, the tail in ε_e creates a tail in the measured Q^2 distribution and thus disturbs the dσ/dt measurement. On the other hand, the θ_e scale can be prepared with high absolute precision. This allows to perform precise T_R scale calibration using the measured θ_e—T_R correlation plots.

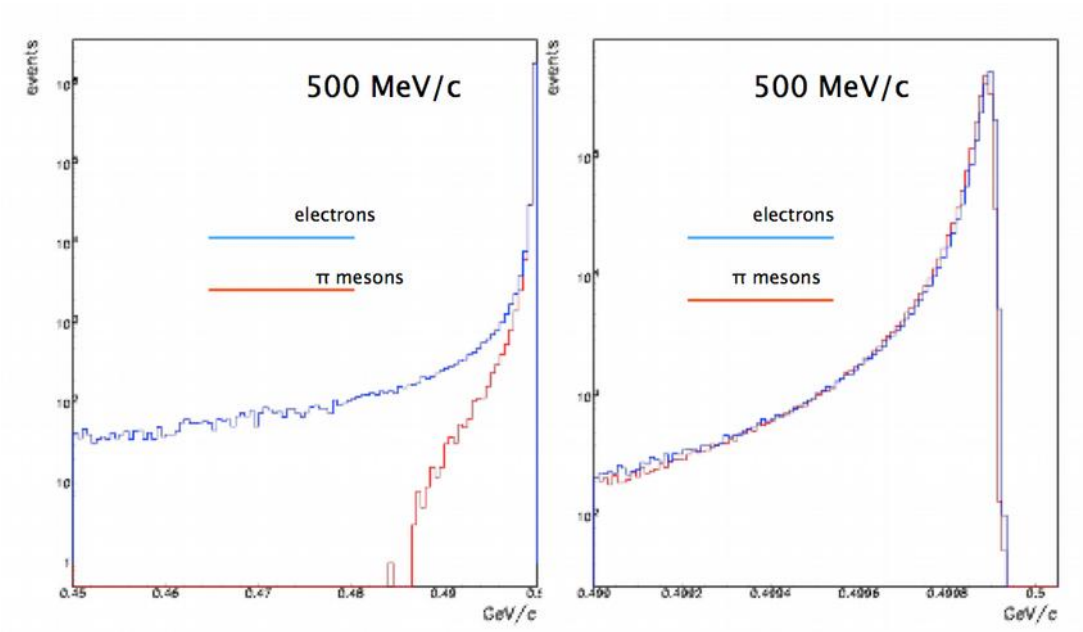

Fig.5. *Energy spectrum of a 500 MeV electron beam after passing 0.5 mm Be window.*

The recoil proton angle θ_R is given by the following expression:

$$\sin(\theta_R) = \frac{(\varepsilon_e + M)T_R}{P_e P_R} \qquad (6)$$

Fig.6 shows dependence of θ_R and θ_e on the recoil proton energy T_R.

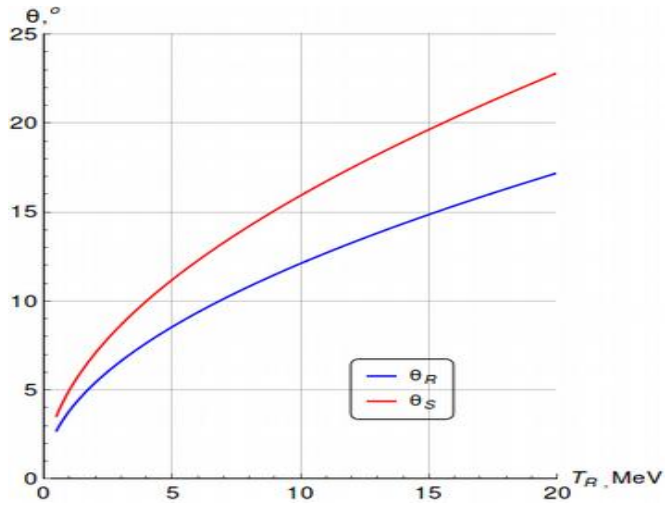

Fig.6. *Scattering electron and recoil proton angles as function of the recoil proton energy for 500 MeV electrons.*

Elimination of the background reactions

The T_R-θ_e , T_R-θ_R, and θ_R- θ_e correlations can be used to eliminate the backgrounds. As an example, Fig.7 demonstrates these correlation plots calculated for the ep elastic scattering and for the background reaction $ep \rightarrow ep\pi^0$ for 720 MeV electrons. One can see that the elastic scattering can be well separated from the background.

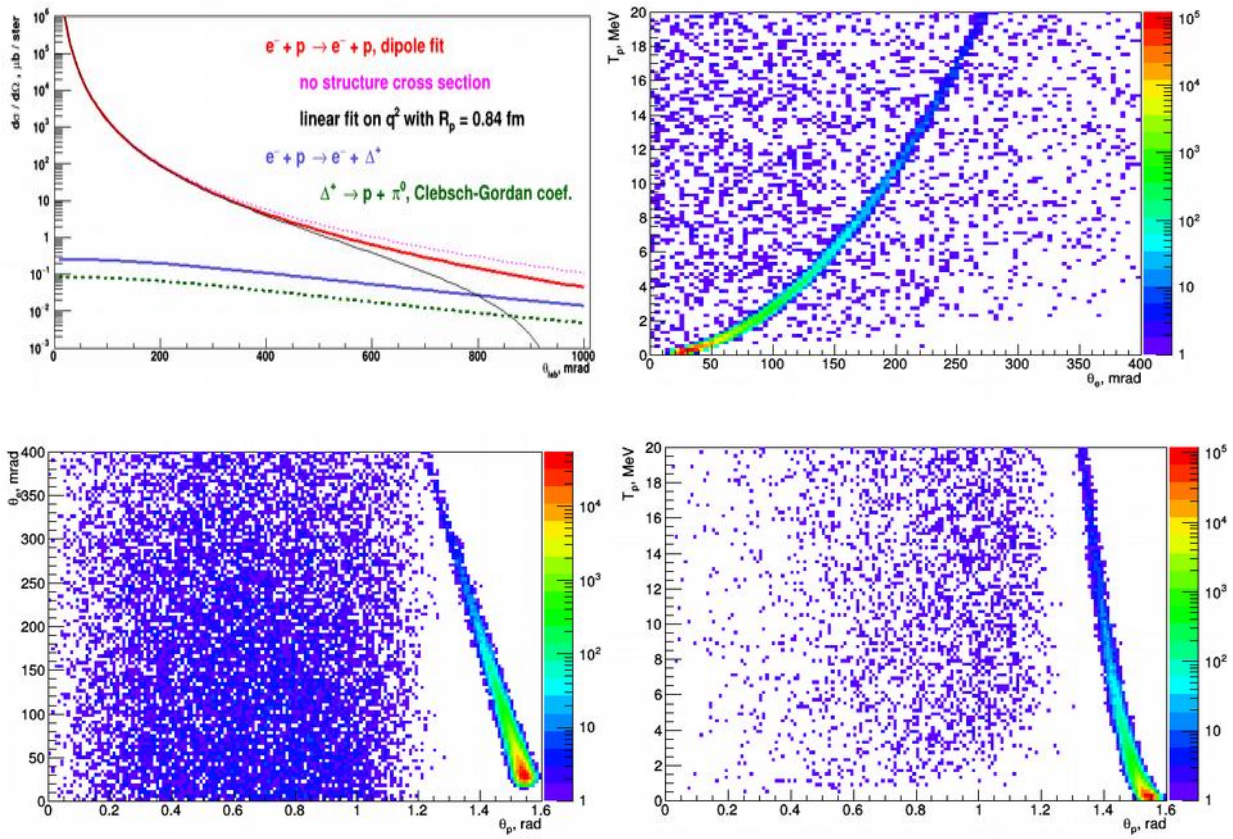

Fig.7. *The T_R-θ_e (upper right), T_R-θ_p (bottom right), and θ_R- θ_e (bottom left) correlation plots calculated for the elastic ep scattering and for the background reaction $ep \rightarrow ep\pi^0$ at ε_e=720 MeV. Also shown the differential cross sections for elastlc and inelastic ep scattering (upper left). Note that θ_p in these plots corresponds to 90^o- θ_R.*

Radiative corrections

Fig.8 shows the main diagrams of the radiative processes in the ep scattering. In the previous experiments, where the transfer momentum was determined by measuring the angle and momentum of the scattered electron, the main contribution to the radiative corrections came from diagrams v2, r1, and r3. These corrections were quite large (δ ~ 10%) and Q^2 dependent. On the contrary, they cancel each other almost exactly when the transfer momentum is determined by the recoil proton method, applied in this project for the first time in the ep scattering experiments.

In our case, the vacuum polarization correction from diagram v1 gives the largest contribution. It can be calculated with high precision as demonstrated in Fig. 9 which shows the results of such calculations made by Andrej Arbuzov specially for our experiment. The corrections enhanced by the large logarithm $\ln(Q^2 m_e^2)$ are cancelled out completely in case of the recoil proton measurements in accord with the Kinoshita-Lee-Nauenberg theorem. The corrections coming from the proton side (v3 ,r3 ,r4) are much smaller being suppressed by the large proton mass. The two photon exchange corrections (v4, v5) can not be calculated from the first principles, though they are believed to be negligible in the low Q2 region. To simulate the effects of radiative corrections, the Monte Carlo generator ESEPP created by the Novosibirsk group will be used. As an example, Fig.10 presents angular distribution of 720 MeV electrons after the ep collision calculated with the ESEPP generator taking into account all radiative corrections. This distribution corresponds to selected recoil energy around T_R=5 MeV. Such calculations can be used to determined the amount of electrons missing the acceptence of our detector (from 20 mrad to 450 mrad). For example, it is ~0.03% for the presented here distribution.

In summary, the radiative corrections in this experiment should be considerably less than in the previous ep scattering experiments. One could expect that these corrections could be calculated to the precision δ ~ 0.1% or better. Moreover, measurements of the absolute differential cross sections in this experiment provide for the first time a possibility to control the level of the calculated radiative corrections.

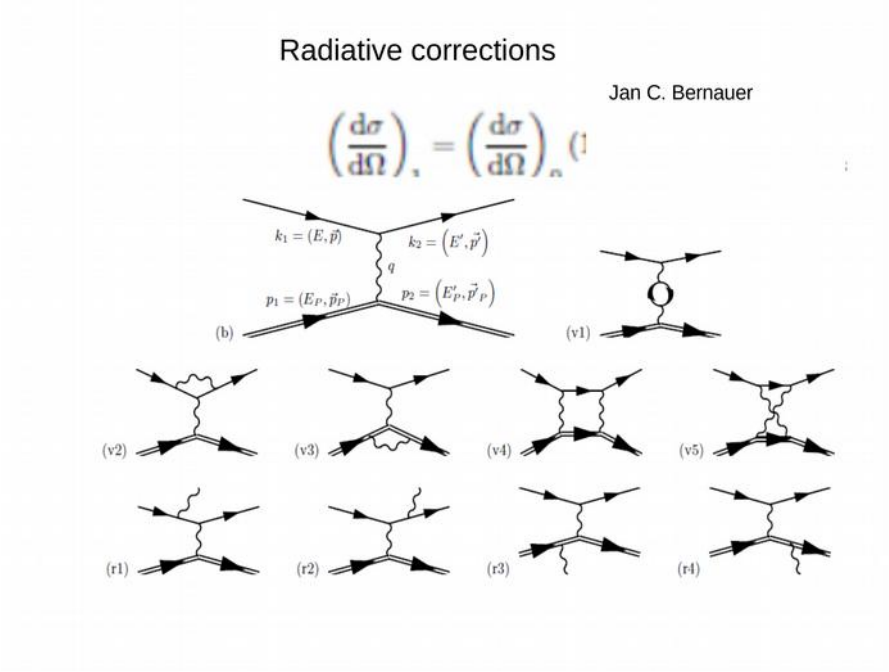

Fig.8 Main diagrams for radiative processes in the ep elastic scattering.

Q^2 GeV²	δ total %	δ lepton %
0.040000	1.76963 (50)	1.70007
0.032941	1.71511(42)	1.65714
0.027128	1.66384 (34)	1.61561
0.022341	1.61546((28)	1.57539
0.018399	1.56960(24)	1.53639
0.015152	1.52605(19)	1.49851
0.012478	1.48444(15)	1.46165
0.010276	1.44452(13)	1.42569
0.008463	1.40607(11)	1.39053
0.006969	1.36889(9)	1.35606
0.005739	1.33279(7)	1.32220
0.004727	1.29760(6)	1.28886
0.003893	1.26318(5)	1.25598
0.003206	1.22941(4)	1.22347
0.002640	1.19618(3)	1.19129
0.002174	1.16342(2)	1.15939
0.001790	1.13104(2)	1.12772
0.001474	1.09898(2)	1.09625
0.001214	1.06721(2)	1.06495
0.001000	1.03566(1)	1.03380

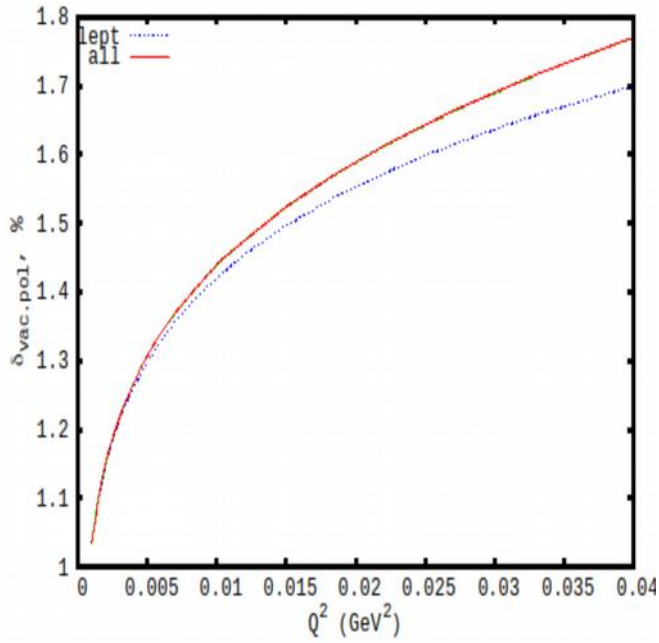

Fig.9 Vacuum polarization corrections for differential cross section of the ep elastic scattering. Correction δ_{lepton} includes only leptonic contribution (electrons, muons, tau-leptons), while δ_{lepton} takes also in consideration the hadronic part.

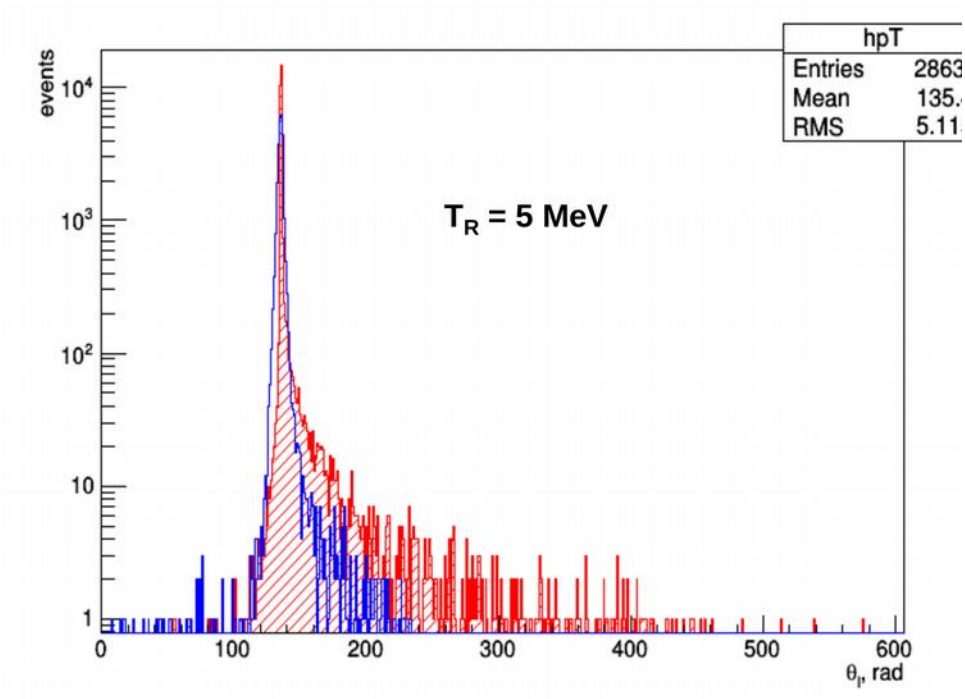

Fig.10. Angular distribution of 720 MeV electrons after the ep collision calculated with the ESEPP generator taking into account all radiative corrections (red colour) This distribution corresponds to selected recoil energy around T_R=5 MeV. For comparison, an angular distribution of the electrons due to multiple scattering is shown (blue colour).

3. Hydrogen Time Projection Chamber

The hydrogen TPC was developed at PNPI, and it has been used in various applications [2,3,4] including experiments WA9 and NA8 at CERN for studies of small angle πp and pp scattering at high energies. The experiment proposed here has much in common with the WA9/NA8 experiments. But there are also essential differences. The absolute precision in dσ/dt achieved in WA9/NA8 was 1%, while in the proposed experiment it should be 0.2%. To reach this goal, some innovations are implemented in the detector design and in the calibration procedures,in particular. Also, the Q^2 range is extended to higher Q^2 region by increasing the hydrogen gas pressure from 10 bar to 20 bar.

In the proposed experiment, the high pressure hydrogen TPC and the large aperture Forward Tracker are placed in one vessel which could stand for pressures up to 25 bar (Figs.11 and 12). These detectors operate with different gas fillings: ultra-clean hydrogen in TPC and Ar+1%CH_4 in the tracker. The TPC volume is separated from the Ar filled space by the walls with a 0.1 mm Be window at the entrance and by a thin Mylar membrane in the downstream wall. The gas pressure in both volumes is permanently equalized. It is foreseen that two gas pressures will be used for the experiment: 20 bar and 4 bar, where the low pressure is used for finer resolution of the lowest Q^2 region. The technical design of the gas circulation/purification system is presented **in Annex 1.**

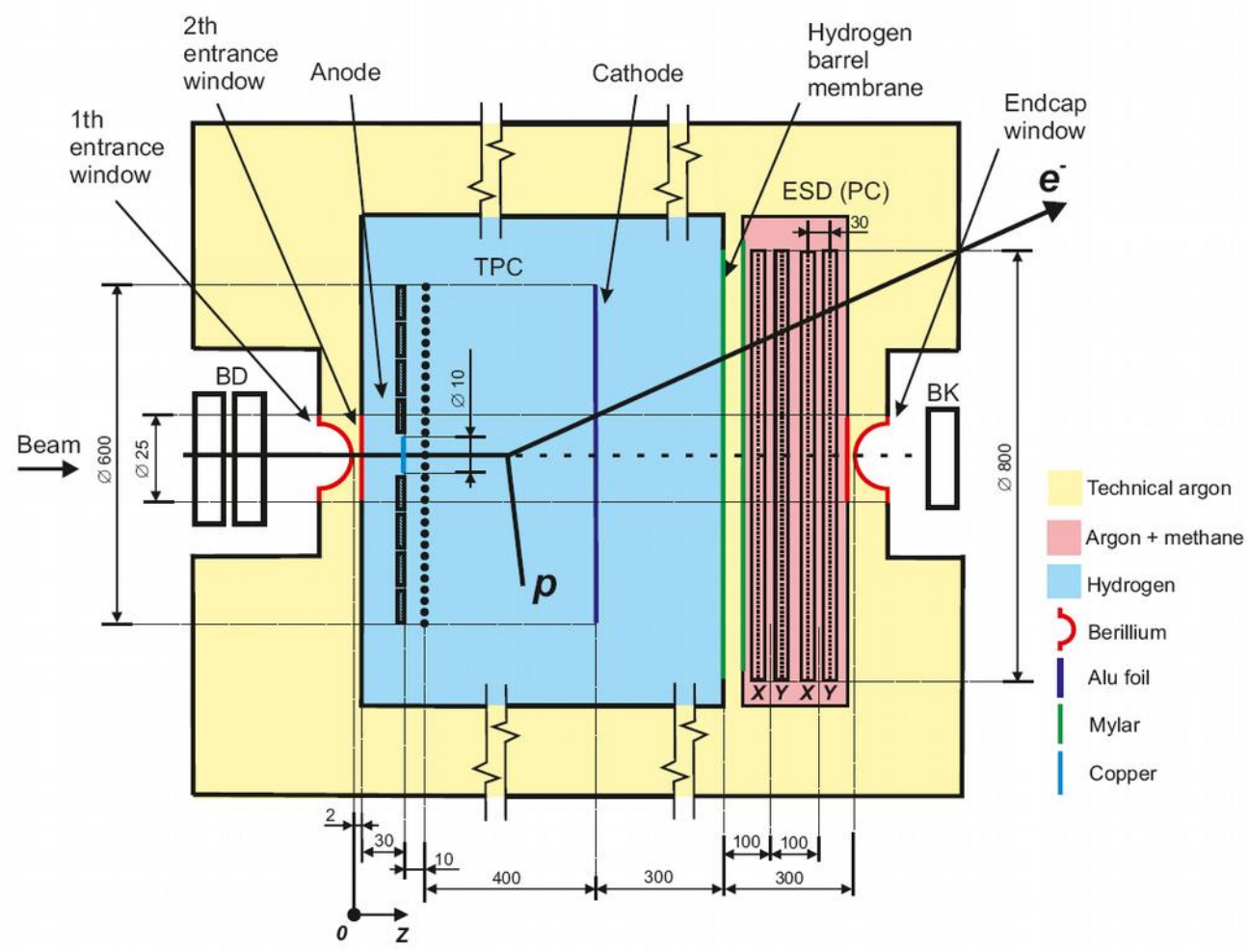

Fig. 11. Schematic view of the TPC & FT detector with three gas volumes

(H2, Ar+1%CH4, and Ar) in a common high pressure vesse

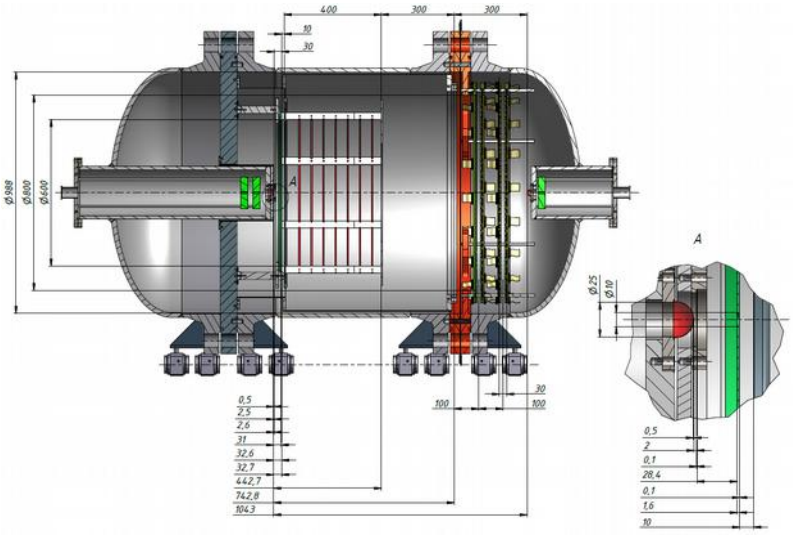

Fig.12. *Tentative design of the combined TPC & FT detector.*

TPC geometry:

Cathode – Grid distance: 400.00 mm ± 40 μm;

Anode – Grid distance: 10 mm;
Grid: 100 μm wires with 1mm spacing. Grid transparency ~2%;
TPC sensitive volume: 600 mm in diameter;
The anode is subdivided into a central pad (10 mm in diameter) surrounded by 7 rings (40 mm width each) plus an outer ring (15 mm width) (Fig.13 left).

Field correction rings are placed in the outer TPC region between the cathode and the grid to form the uniform electric field in the drift space.

TPC will operate at two gas pressures, 20 bar and 4 bar, with the maximal energy of the protons stopped in the TPC sensitive volume 10 MeV and 4 MeV,respectively.

For protons with large energies, TPC measures the remaining energy (for example, 5 MeV for 20 Mev protons at 20 bar H_2) and the angle. Also, there is a possibility to use the CH_4 gas filling. In this case the maximal energy of the stopped inside TPC protons is extended up to 25 MeV (Fig.13 right).

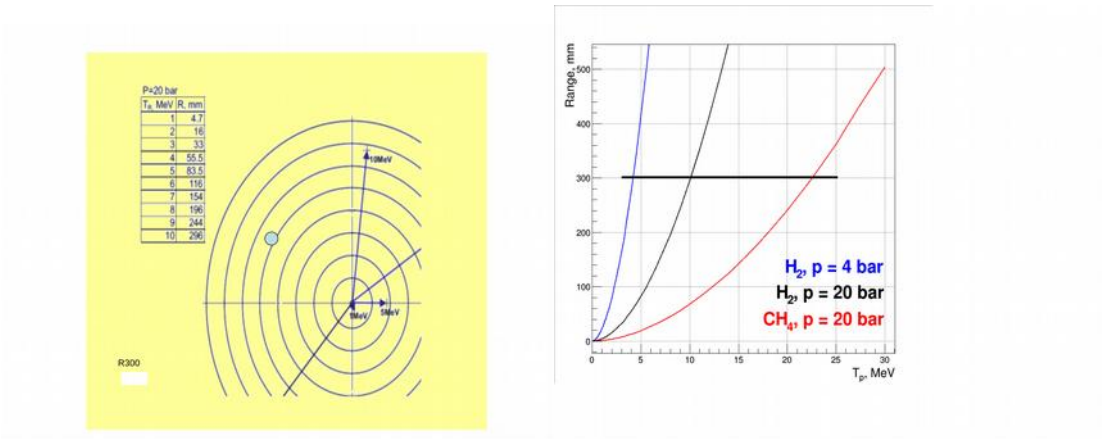

Fig. 13. *TPC anode structure: 10 mm in diameter circle surrounded by 8 rings (Left panel). Proton range-energy plots for H2 gas (20 bar and 4 bar) and for CH_4 (20 bar) (Right panel).*

H_2 gas purity

In order to avoid the losses of the ionization electrons during the drift time, the contamination of the H_2 gas by any electro-negative gas (O_2, H_2O) should be reducedto a level below 1 ppm. This will be achieved by continuous H_2 purification with a special gas purification system, similar to that described in [5], which eliminates gas impurities down to **< 0.1ppm.** (Details in **Annex 1).**

H_2 atomic density

The number of protons per cm^3, n, in hydrogen gas as a function of pressure, P_{tech}, and temperature, t^0, is given by the following expression:

$$n = 5.2005 \cdot 10^{19} \cdot P_{tech} \cdot 273.16 \ / (1 + 0.000524\ P_{tech})\ (273.16 + t^0), \qquad (7)$$

where P_{tech} = 735.552 mmHg.

In our experiment, pressure will be controlled to **0.01%** absolute precision and temperature will be kept constant with **$\pm 0.05^0$** **(0.014%** absolute precision). This determines the proton density with **0.025%** absolute precision.

Time, recoil energy, and recoil angle resolution

The anode channels will be equipped with low noise preamplifiers with the noise at the level of **20 keV (sigma).** This determines the recoil energy resolution. Depending on the range of the recoil proton, the recoil energy is obtained by the sum of energies deposited against the anode rings. Accordingly, the noise will be summed up as well. So the energy resolution, depending on the number of the rings crossed by the proton, is varied from 20 keV to 55 keV for maximal proton range (T_R~ 10 MeV for 20 bar, T_R~ 4 MeV for 4 bar).

The expected signal arrival time resolution is **40 ns (sigma).** The angular resolution in θ_R is limited by the Coulomb scattering of the recoiled protons: ~ 10 mrad (sigma).

θ_R is measured by the differences in arrival times of the signals from the anode rings crossed by the recoil (this is possible for tracks exceeding 60 mm, that is detected by at least two anode rings). The precision of such measurements varies from ~ ±10 mrad (signals from two neighbor rings) to ~ ±2 mrad for long ranged protons.

So the final recoil angle resolution will be **from 15 mrad to 10 mrad** (for proton range 60-80 mm and ~ 300 mm, respectively).

Note, however, that the noise might be larger in the presence of the electron beam.

This problem was investigated in the test experiment performed in August-September 2017 in the MAMI electron beam using an available TPC prototype filled with He + 4% N_2 gas mixture up to 10 bar pressure. According to our MC calculations, the ionization properties of this gas mixture are close to that of pure hydrogen (which could not be used in this run because of safety requirements). The details of this experiment are presented **in Annex 2**. The obtained results proved to be in reasonable agreement with the MC simulation. The conclusions from these measurements and MC simulations are as follows:

* The beam introduces additional “beam ionization noise” mostly on the central 20 mm in diameter anode pad;
* The beam noise is increasing with beam rate as root square of the rate up to 60 keV at 1.6 MHz beam rate (10 bar gas pressure);
* The beam noise is nearly proportional to the gas pressure;
* The beam noise is increasing slightly with the total drift gap;
* The beam noise is increasing slightly with the drift velocity.

Based on these results , we can use the MC model for prediction of the beam noise conditions in our main experiment. The results are presented in Fig. 14.

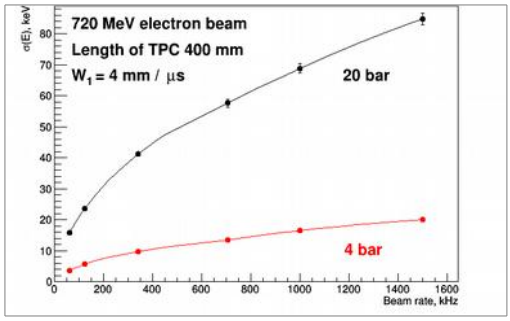

Fig.14. MC prediction of the beam ionization noise on the central pad for the main experiment. Pure hydrogen. 20 bar and 4 bar gas pressure. Drift gap 400 mm. Drift velocity 4 mm/μs.

Electron drift velocity and track diffusion in TPC

The electron drift velocity is $W_1 \approx 0.42$ cm/μs in the TPC drift region and $W_2 \approx 0.75$ cm/μs in the region anode-grid. The value of W_1 should be known with high precision (better than 0.1%) as it determines the selected gas target thickness (important for absolute dσ/dt measurements) and determines the Z-coordinate of the vertex used to measure θ_e.

The value of W_1 will be measured in special measurements by detecting time intervals between the beam trigger and the signals produced by the beam electrons crossing TPC perpendicular to the TPC axis at three Z- coordinates counted from the the HV plane: Z=10 mm, Z=200 mm, and Z=380 mm. Three Be windows in the TPC body will be arranged at these distances. The whole setup should be turned by 90 deg for these measurements (Fig.15). The distances between the selected Z- coordinates will be determined with 20 μm precision by precision shifting the setup across the beam direction. Note that the beam intensity should be reduced to 10^4 e/sec to exclude the overlapping signals in TPC. The expected precision in measurements of the drift velocity is **0.01%.**

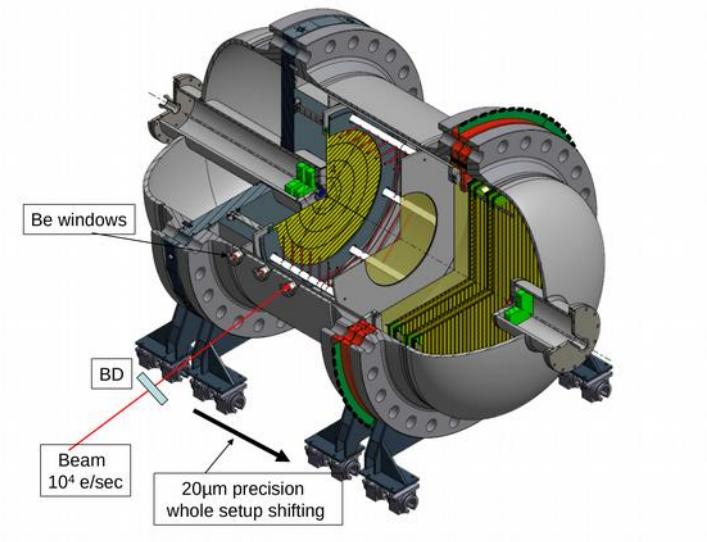

Fig.15. *Experimental layout for high precision measurement of electron drift velocity.*

The same measurements will provide information on track diffusion during the drift time by observation of the TPC signal width in function of the drift time. According to the available

literature information [6], the track diffusion is rather small. In our experimental conditions it should be $\sigma_L \approx 0.006 \sqrt{L}$, that is **~ 400 μm (sigma)** for maximum drift distance L=40 cm. The diffusion is not important for measurements of W_1 where arrival time will be determined by the signal maximum. But it may have some effect on measurement of arrival times of the TPC signals which will be determined by the front-edge of the signals. In this case some small corrections to the measured arrival times may be needed. The magnitude of these corrections will be obtained in the diffusion measurements, mentioned above.

The drift velocity depends on the E/P (electric field / pressure) ratio in the drift space. The change in E/P by 1.5% changes W by 1%. In our experiment, both HV and the pressure will be kept stable and reproducible **on a level of 0.01%.** The W measurements will be performed at HV=100kV, 95kV, and 90kV. Similar measurements will be performed at 4 bar pressure with HV reduced by a factor of five.

Gas target length

The gas target length, L_{tag}, is determined from the measured difference between maximal and minimal arrival times of the TPC signals in the chosen drift space, $L_{tag} = (t_{arr\ max} - t_{arr\ min}) \cdot W_1$. Only a small correction to $t_{arr\ max}$ might be needed for track diffusion. The expected precision in L_{tag} determination is **0.02%** for L_{tag}=35 cm.

Vertex Z coordinate. Calibration and resolution.

The knowledge of the vertex absolute Z-coordinate is needed for measurement of the electron scattering angle. Calibration of the Z-scale will be done simultaneously with measurements of the drift velocity. The TPC setup will be slightly turned so that the electron beam (in position Z=10 mm) will cross the HV plane in the TPC central region thus producing ionization at Z close to Z=0. Registration of these signals can fix the Z scale in TPC with absolute precision **better than 100 μm**. Note that the electronics delays between the beam trigger and TPC signals should be identical to those in the main experiment.

Another way to determine Z = 0 can be detection of the signals produced by the beam electrons on the central anode in the nominal zero degree TPC position. The Z=0 point can be found by analyzing the end part of these ~ 100 μs long signals. Advantage: such measurements can be done at any time in the course of the main experiment (with beam intensity reduced to 10^3 e/sec). The main disadvantage is relatively large systematical uncertainty in determining the Z=0 point. The optimal solution would be calibration of this method by the 90 degree setup measurements. Then it can be used as a stability control for the Z scale calibration in the course of the experiment.

As to the Z resolution in detection of the recoil protons, it depends on the arrival time resolution. The Z-resolution is expected to be **σ_z ~ 200 μm.**

4. Forward Tracker

The Forward Tracker is designed for high absolute precision in measuring the X and Y coordinates of the electron track relative to the beam line. Also, it provides fast signals for the trigger system. The FT consists of two pairs of Cathode Strip Chambers X_1/Y_1 and X_2/Y_2. Each chamber is a symmetric MWPC with 2.5 mm gap between the cathode and the anode planes. The size of the chamber is 600x600 mm^2. The readout is from both cathode planes. The anode wire plane will contain 30 μm wires spaced by 3mm. Both cathode planes are made with 100μm (or 50 μm) wires wound with 0.5 mm step. The cathode wires are orthogonal to the anode wires in one cathode plane and inclined by 45 deg. in the other cathode plane. The wires in the inclined cathode plane are grouped into 10 mm strips.

The key element of the CSC is the cathode plane with orthogonal cathode/anode wires. It determines the absolute measurements of the coordinate along the anode wire. In this plane, 2 mm strips will be formed by joining together 4 wires. The width of all strips should be identical within ± 20 μm. This allows determination of the center-of gravity of each detected signal with a precision ~1% of the strip width (σ_{proj}~ 30 μm) assuming the signal to noise ratio S/N > 100 and the electronics amplification uniform within 1% in each readout channel. The most important requirement to the strip plane is that it should provide absolute linear scale with ~0.02% precision. We plan to reach this goal by developing high precision wiring and by final certification of the wire strip positions with a microscope.

To obtain the ratio S/N ≥ 100, the CSC gas gain should be ≥10^3. It is not trivial to obtain such gain at 20 bar pressure with 600 mm long anode wires. In particular, it is not possible in pure hydrogen. That is why we shall use Ar +CH_4 gas mixture.

There will be a dead zone in the centers of the CSCs (~ 20 mm in diameter) to reduce the sensitivity to the electron beam crossing the CSCs. This will be done by electrolytically depositing an additional gold layer on the anode wire in this spot. Note that some sensitivity still will remain, and it will be used in the CSC alignment procedure.

. A special CSC prototype has been constructed at PNPI and tested with high gas pressures up to 20 bar. It was demonstrated that the required gas gain can be reached in the designed CSC. The details are presented in **Annex 3.**

5. Beam detectors

The beam detectors have several functions:

- Tracing the beam line and control for beam stability
- Measuring the arrival times of the beam electrons
- Absolute, high precision counting of the incoming beam electrons for determination of the absolute cross section.

The first of these functions is provided by the Pixel detectors which were successfully tested in the 2017 test run. (3x3 mm^2 size, 80x100 μm^2 pixels).
The second and the third functions could be realized by two thin ultra-fast scintillator detectors placed upstream of the TPC&FT detector. These detectors constructed and tested in the 2018 test run.

6. Trigger and acquisition

The choice of the trigger is one of the critical points in the experiment. Fortunately, we have possibility to use the TPC recoil proton signals for triggering the readout system. This is the most safe and effective triggering option.

As it was demonstrated in the test run, the background in TPC produced by the electron beam is rather low. The self-trigger rate from TPC operating at 10 bar pressure was ~ 8Hz at the beam intensity 1.6 MHz, the trigger being defined as any signal exceeding the 300 keV level in any of 66 anode pads. Most of this rate is due to elastic e^{4}He scattering (~3.5 Hz) and from inelastic reactions on ^{4}He and Nitrogen. That means that in the main run with hydrogen in TPC, the self trigger rate would be determined mostly by the ep elastic scattering events. The expected rate of such events is $N_{ep\_elastic}$ = 30 Hz with the threshold set at 300 keV at P=20 bar and 6 Hz at P=4 bar.

Based on these obsevations, the acquisition system has been designed. It will use continuous data flow and can operate at mean TPC self-trigger rate 50 Hz without introducing any dead time. After receiving a trigger signal, the information from all detectors appeared in a regulated time interval (up to 655 μs) before arrival of the trigger is readout from the pipeline and sent to DAQ. The details are presented in **Annex 4**. The efficiency in detection of the ep events triggered by the TPC self-trigger in the measured t-range should be close to 100%.

The measured quantities are presented in the Table.

	Measured quantity
1	Recoil proton energy
4	Time arrival of TPC signals
5	X & Y coordinates in CSCs
6	Time arrival of CSCs signals
8	Time arrivals of beam detectors signals

6. Alignment

High precision alignment of various parts of the detector is needed for precision measurements of the electron scattering angle θ_e. Fig.12 presents a tentative design of the TPC@FT detector. In this design, the entrance flange is used as a reference plane in the alignment procedure:

- The TPC anode plane, grid plane, HV planes, and the plane of the block of CSCs will be set to be parallel to the entrance flange plane to **0.1 mrad precision**.
- Z distances between the TPC HV plane and the anode wire plane in each CSC as well as Z distance between the TPC HV plane and the TPC grid plane will be measured to **40 μm precision**.
- The whole detector should be installed in such a way that the entrance plane will be strictly **(± 0.1 mrad)** perpendicular to the beam line. This procedure is not fixed yet, to be discussed with MAMI experts.
- Only modest precision (± 1mm) in the X/Y alignment of CSCs is foreseen. The precise X=0, Y=0 position in CSCs will be measured by the beam tracing. The pixel detectors will determine the beam line while CSCs (in coincidence with Pixels) measure the X=0, Y=0 coordinates with **better than 20 μm precision.**

The final control for the X=0, Y=0 position and for the angle between the detector planes and the beam axis will be done by the azimuthal symmetry analysis of the experimental data.

7. Azimuthal symmetry

In case of ideal alignments (that is when the electron beam is strictly perpendicular to the detector planes and crosses CSCs at X=0,Y=0), the azimuthal distributions of the detected events in the X-Y plane should be ideal circles at any θ_e. If the beam is displaced by ΔX (ΔY), this will shift the centers of the circles by ΔX(ΔY) relative to the initially chosen center (X=Y=0), independently on θ_e. On the other hand, the appearance of some angles φ_X (φ_Y) between the beam direction and the XZ (YZ) planes in CSCs will produce shifts proportional to $\varphi_X \cdot z \cdot (tg\theta_X)^2$ and $\varphi_Y \cdot z \cdot (tg\theta_Y)^2$, where z is the distance from of the ep vertex to the CSC anode plane. Fitting the experimental data with $\Delta X + \varphi_X \cdot z (tg\theta_X)^2$ and $\Delta Y + \varphi_Y \cdot z \cdot (tg\theta_Y)^2$, one could find ΔX, ΔY, φ_X , and φ_Y with estimated precision **± 20 μm** for ΔX(ΔY) and **± 0.1 mrad** for φ_X, and φ_Y. Note that the misalignments of this level has negligible effect on the measured θ_e distributions due to averaging over the whole azimuthal space.

8. Calibration of the t-scale

The critical point in the recoil proton method is extraction of the t-value from the observed TPC signal, S_{TPC}. One should take into account not only dependence of the produced ionization on the energy of the recoil proton but also several other factors: recombination, lost of electrons in the drift space (attachment to O_2), grid transparency, shaping of the signal. Moreover, these effects depend on experimental conditions. The best way to solve this problem is to perform calibration of the TPC signals directly in the experimental setup.

The calibration of the TPC t-scale foreseen in this experiment relates the observed signals S_{TPC} with the absolute t-values determined from the measured θ_e distributions.

The calibration will be done using collected real experimental data. For that, we select a bin ΔS_{TPC} in the 2D plot S_{TPC} - θ_e and look at the corresponding θ_e distribution. This will be a peak at θ_{eM} with a tail to larger angles due to the energy losses of the electron before the ep collision. However, the maximum of the spectrum at θ_{eM} (with corrections for the energy losses before the ep collisions) should correspond to the undisturbed incident beam energy ε_e thus allowing to determine the t-value corresponding to the selected S_{TPC} bin. This procedure is illustrated in **Annex 5**.

The main statistical error in determination of θ_{eM} comes from the electron multiple scattering. This leads to the θ_e dispersion ~1 mrad (sigma) at 500 MeV in the electron detector region. However, the θ_{eM} position could be determined with 0.01mrad (sigma) around T_R =1MeV and with 0.02 mrad precision around T_R =10 MeV due to high statistics ($>10^5$ and $>10^4$ in each bin, correspondingly). Our θ_{eM} range goes from 85 mrad (T_R = 1MeV) to 270 mrad (T_R = 10 MeV) at 500 MeV**.** That means that the statistical error in θ_{eM} will be **on a level of 0.01%** in the whole T_R range.

To determine the absolute t-value, one should know the absolute values of θ_{eM} and ε_e. As to the absolute beam energy ε_e, it is known at MAMI with ± 120 keV at 720 MeV and with ± 140keV at 570 MeV, that is with **~ 0.02%** precision. The absolute precision in measurement of θ_{eM} is determined mostly by the liniar scale in the CSC strip planes, and it is expected to be **0.02%** in the whole t-range from 0.002 to 0.04 GeV^2. Adding these two errors linearly, we can expect **0.08%** precision in absolute TPC t-scale calibration**.**

This procedure should be done for several intervals in the vertex Z positions to determine corrections for possible Z dependence of the TPC signals at fixed recoil proton energies.

9. Statistics and beam time

The statistical error in the measured proton radius was estimated by simulation of $3.3\cdot10^7$ ep scattering events in the t-range from 0.002 GeV^2 to 0.04 GeV^2. Such number of events could be collected during 45 days of continuous running with $2\cdot10^6$ e/sec beam with TPC operating at 20 bar with target thickness $3.6\cdot10^{22}$ protons/cm^2 (L_{target} = 35 cm). The differential cross section with dipole form factors was used for simulation of the ep elastic scattering events. The fit was done with a Q^4 term included in the form factor. The results are presented in Fig.16. The statistical error proved to be σ(Rp) =0.005 fm without normalization of the simulated data. This error might be reduced in our case of measured cross sections with normalization error of ±0.2%. Also, it can be reduced by extanding the t-range down to 0.001 GeV^2.

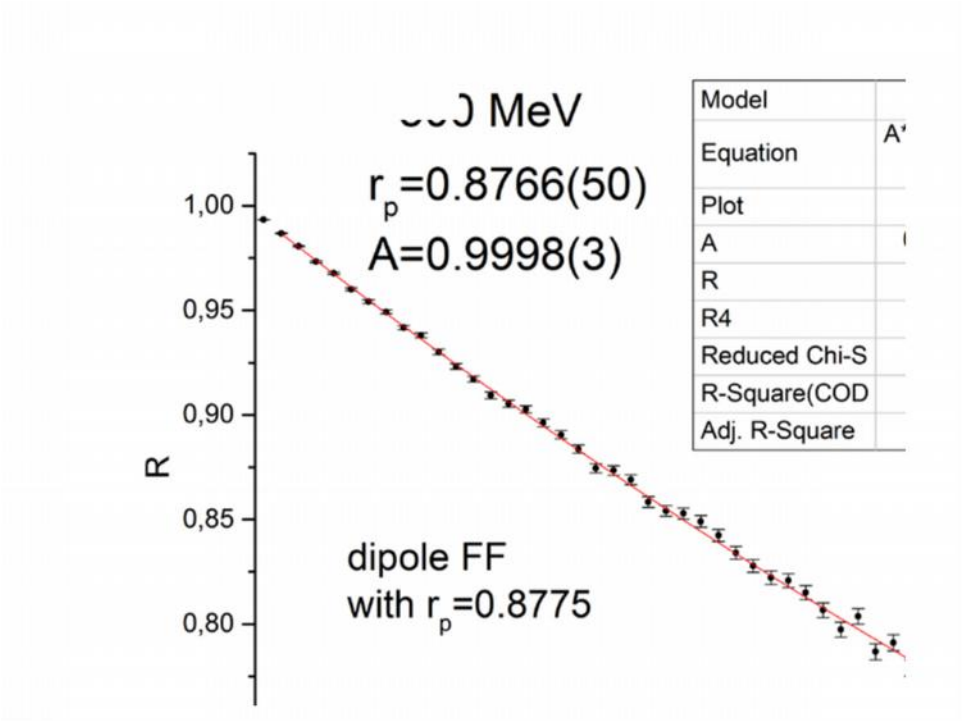

Fig. 16. *Simulation studies of statistical error in measurement of the proton radius.*

10. Systematical errors in measurements of dσ/dt.

The possible systematical errors were discussed in the text above. These errors are summarized in Table 2. Also shown how these errors contribute to the errors in dσ/dt. One can see that the systematical errors are 0.1 % in the relative measurements of dσ/dt and 0.2% in the absolute measurements, which corresponds to the declared goal of this experiment.

Table 2. The systematical ***errors entering the measured dσ/dt***

		Syst. Error %	comment
1	Drift velocity, W1	0.01	
2	High Voltage, HV	0.01	
3	Temperature, K	0.015	
4	Pressure, P	0.01	
5	H_2 density , ρ_p	0.025	Sum of errors 3 and 4
6	Target length, L_{tag}	0.02	
7	Number of protons in target, N_p	0.045	Sum of errors 5 and 6
8	Number of beam electrons, N_e	0.05	Clean Tr0 free of pileups
9	Detection efficiency	0.05	
10	Electron beam energy, ε_e	0.02	
11	Electron scattering angle, θ_e	0.02	
12	t-scale calibration, T_R relative	0.04	Follows from error 11
13	t-scale calibration, T_R absolute	0.08	Follows from the sum of errors 11 and 10
	dσ/dt , relative	0.1	0.08% from error 12
	dσ/dt , absolute	0.2	0.16% from err.13 plus errors 7,8,9

11. The layout of of the experimental setup

The TPC&FT detector will be installed on the rails on a platform of 1.5m x 2.5m size (Fig.17). The detector can be moved along the rails for 400 mm under 20 μm precision control. The platform stands on three legs allowing smooth regulation in height. The legs have air pillows which allows tuning the detector position relative to the beam line.

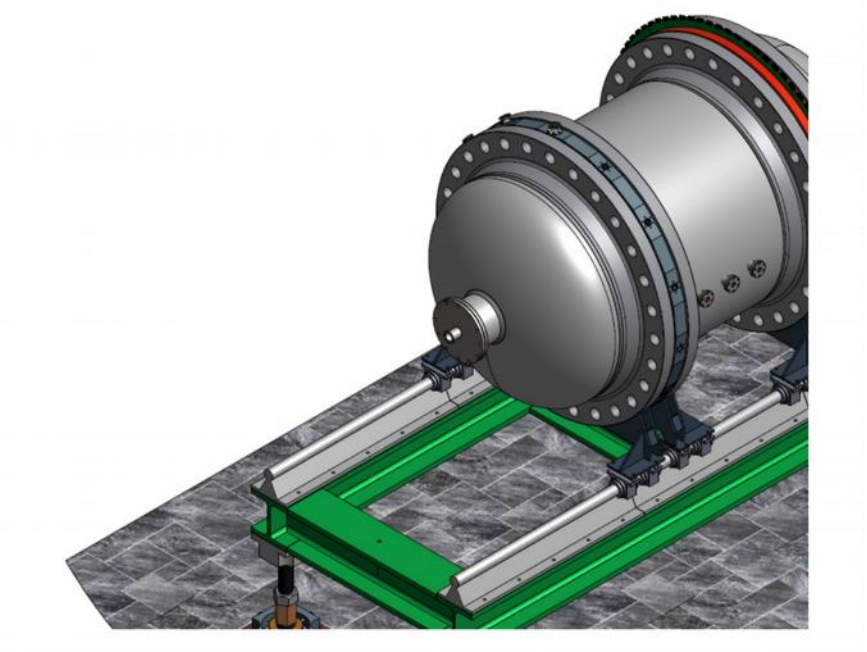

Fig. 17. *The TPC&FT detector on a movable platform.*

Fig. 18 shows a layout of the TPC&FT detector with corresponding infrastructure (the gas circulation/purification system, the high voltage system, the acquisition system etc.). All these systems will be placed into five racks. These racks could be installed in arbitrary place within 10 m distance from the TPC&FT detector. All communication lines from the racks to the detector will go via a vertical support allowing to turn the detector by 90 degrees without dismounting the communication lines. The total area occupied by the TPC&FT detector is 3 x 3 meters. The body of the TPC&FT detector will be covered with a thermo-shirt with temperature stabilization $\pm 0.05^0$.

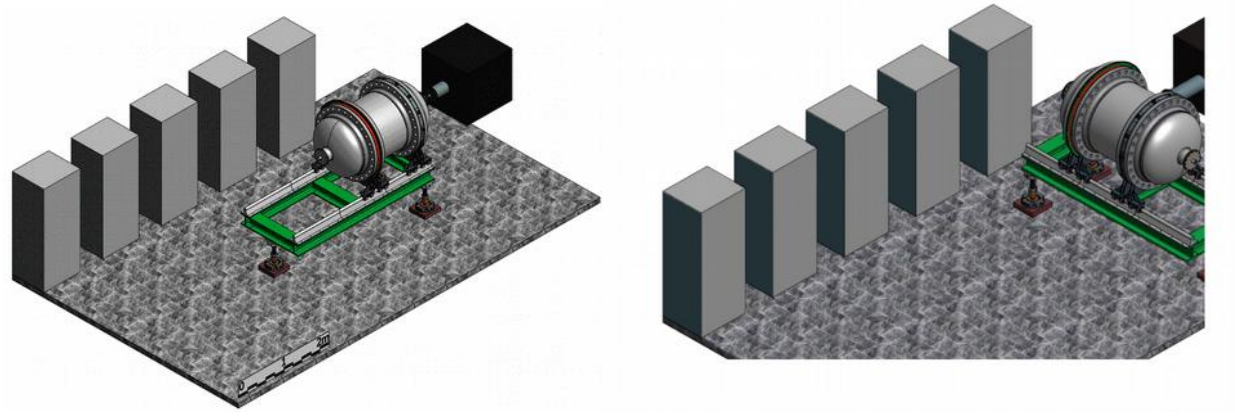

Fig.18. *Experimental layout for the physics run (left) and for drift velocity measurements (right).*

12. The working plan

2018

In the fall of 2018, we plan to repeat a test experiment with the 720 MeV electron beam at MAMI with the same active target as in the 2017 test run but filled with hydrogen.The active target used in the previous test run was filled with the $^4He+4\%N_2$ gas mixture because of restrictions to use hydrogen for the setup available by that time.

For the next run a special equipment will be produced and installed which satisfies the safety requirements. This equipment includes a lodge covering the whole setup (Fig.19) and a safety pressure release system (Fig. 20). Note that this equipment, being tested in the test run, will be later used in the main experiment.

Another task for this test run is to complete testing of the beam detecting system so that it could be ready for the main experiment.

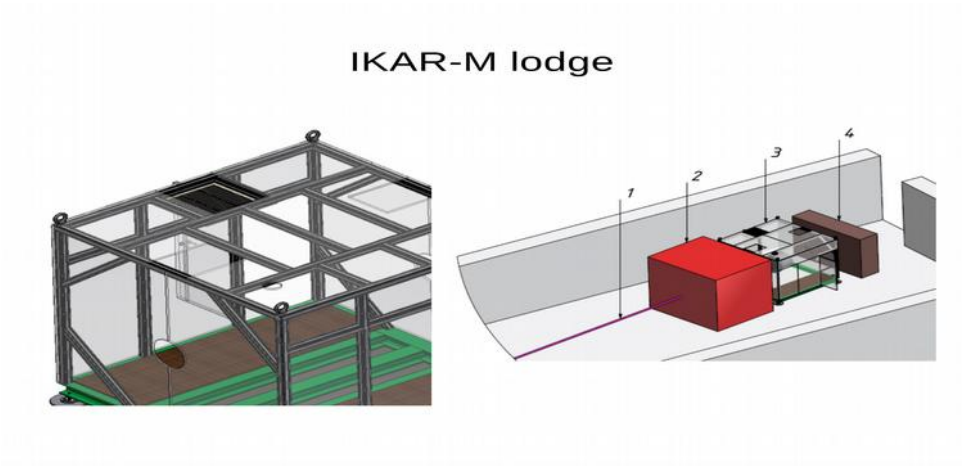

Fig. 19. Designed safety lodge covering the FTC&FT setup.

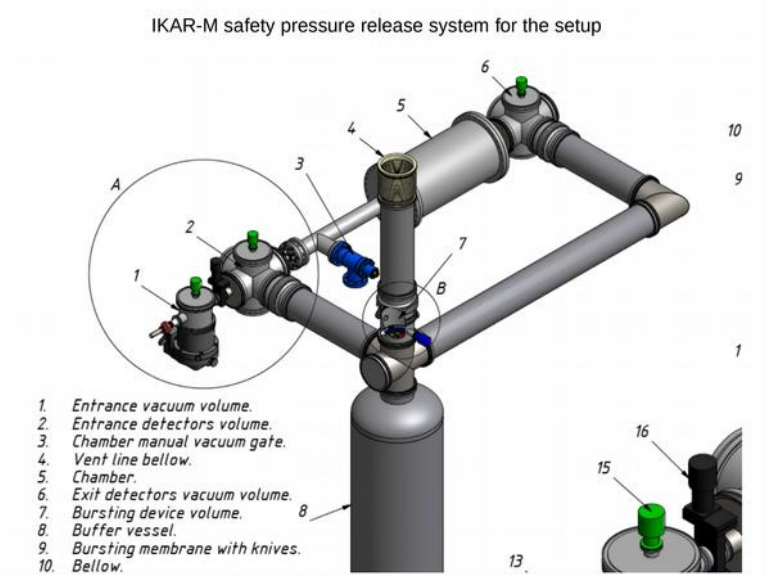

Fig.20. Safety pressure release system for the TPC&FT setup.

2019

By mid of 2019 the TPC&FT detector with infrastructure will be ready for installation. We plan to install the whole setup in the experimental area in the fall of 2019 and make some preliminary tests in the 720 MeV beam.

2020

Physics run with the 720 MeV beam.

14 . Beam requirements

MAMI Specifications

Beam energy	720 MeV
Energy spread	< 20 keV (1σ)
Energy shift	< 20 keV (1σ)
Absolute energy	±< 150 keV (1 σ)

Electron Beam Specifications

Beam intensity (main run)	2x10^6 e/sec
Beam intensity for calibration	10^4 e/sec and 10^3 e/sec
Beam divergency	≤ 0.5 mrad
Beam size	minimal at given divergence

References:

1. Conference at Trento, June 2016. http://www.ectstar.eu/node/1659.

2. Soft πp and pp scattering in the energy range 30 to 345 GeV. Experiments WA9/NA8 at CERN.
J.P. Burq *et al*. Nucl. Phys.B 217 (1983) 285-335.

3. Study of nuclear matter distribution in neutron-rich Li isotopes. Experiments at GSI.
A.V. Dobrovolsky *et al*. Nucl.Phys.A 766 (2006) 1-24.
Precision measurement of the rate of muon capture in hydrogen gas and determination of the proton pseudoscalar coupling. Experiment MuCap at PSI. V.A. Andreev et al. Phys.Rev.Lett. 110, 022504 (2013).

4. A circulating hydrogen ultra-high purification system for the MuCap experiment.
V.A. Andreev *et al*. NIM A578 (2007) 485.

5. Theory of Electron Diffusion Parallel to Electric Fields. II. Application to Real Gases.
J.J. Lowke and J.H. Parker Phys.Rev. v181 № 1 (5 May 1969).

\